



Improving mathematical model of burden distribution and correcting chute angle to cope with fluctuation of stock line

Jian-sheng Chen¹ · Wen-guo Liu¹ · Hao Guo² · Wang Ding³ · Qing-guo Xue¹ · Jing-song Wang¹ · Hai-bin Zuo¹

Received: 31 December 2022 / Revised: 3 April 2023 / Accepted: 6 April 2023 / Published online: 11 August 2023
© China Iron and Steel Research Institute Group Co., Ltd. 2023

Abstract

Accurate evaluations of the burden distribution are of critical importance to stabilize the operation of blast furnace. The mathematical model and discrete element method (DEM) are two attractive methods for predicting burden distribution. Based on DEM, the initial velocities of the pellet, sinter, and coke were calculated, and the velocity attenuations of the above three particles between the burden and the chute were analyzed. The initial velocity and velocity attenuation were applied to a mathematical model for improving the accuracy. Additionally, based on the improved model, a scheme for rectifying the chute angles was proposed to address the fluctuation of the stock line and maintain a stable burden distribution. The validity of the scheme was confirmed via a stable burden distribution under different stock lines. The mathematical model has been successfully applied to evaluate the online burden distribution and cope with the fluctuation of the stock line.

Keywords Burden distribution · Mathematical model · Discrete element method · Velocity attenuation · Stock line fluctuation

List of symbols

d	Diameter of feeding pipe, m	l_{β}	Effective length of chute, m
D_0	Diameter of throat, m	L	Falling point of burden in furnace, m
e	Vertical distance from suspension point to bottom of chute, m	L'	Falling point of burden at low stock line, m
g	Gravitational acceleration, m/s^2	r	Radial position of burden in furnace, m
h_0	Height of empty zone, m	R	Radius of throat, m
h_1	Height of stock line, m	$f_1(r)$	Function of old burden profile
h_2	Distance from end of chute to throat, m	$f_2(r)$	Function of new burden profile
H_0	Distance from throttle valve to suspension point of chute, m	t	Falling time of burden into empty zone, s
H_h	Height of throat, m	v_{0C}	Initial velocity of coke, m/s
H_s	Height of stack, m	v_{0P}	Initial velocity of pellet, m/s
k	Attenuation coefficient of velocity	v_{0S}	Initial velocity of sinter, m/s
l	Length of chute, m	V_c	Calculated charging volume, m^3
		V_r	Real charging volume, m^3
		w_c	Batch mass of coke, kg
		w_o	Batch mass of ore, kg
		α	Chute angle, ($^{\circ}$)
		β	Incident angle of particle, ($^{\circ}$)
		β'	Rebound angle of particle, ($^{\circ}$)
		β_s	Angle of stack, ($^{\circ}$)
		γ	Opening of throttle valve, ($^{\circ}$)
		ε	Volume tolerance
		μ	Friction coefficient of burden
		μ_c	Friction coefficient of coke
		μ_s	Friction coefficient of sinter

✉ Hai-bin Zuo
zuohaibin@ustb.edu.cn

¹ State Key Laboratory of Advanced Metallurgy, University of Science and Technology Beijing, Beijing 100083, China

² MCC Capital Engineering & Research Incorporation Limited, Beijing 100176, China

³ Hunan Valin Xiangtan Iron and Steel Co., Ltd., Xiangtan 411101, Hunan, China

ρ_c	Packing density of coke, kg/m ³
ρ_o	Packing density of ore, kg/m ³
ω	Rotational speed of chute, rad/s

1 Introduction

The rising economic competition and environment protection problem are main challenges faced by the steel-making industry, as CO₂ emissions must be dramatically reduced in the future. One of the several obstacles hindering the CO₂ mitigation process is the insufficient efficiency improvement of the ironmaking blast furnaces because of its heavy dependence on coal or coke as the primary reductant and energy source [1]. Improving the energy efficiency to minimize the consumption of reducing agent is an important method to reduce CO₂ emissions in blast furnaces. Burden distribution within a blast furnace is directly related to the gas distribution, heat transfer and chemical reactions inside the furnace, which further affects the shape and position of the cohesive zone. An appropriate burden distribution is a prerequisite for the full utilization of energy, reducing CO₂ emissions, and the stable operation of the blast furnace. Therefore, accurate predictions of the particle trajectory, falling point, and burden distribution are of critical importance to design and optimize the charging system of the blast furnace. Various methods, such as physical experiments [2–5], data-driven approaches [6], mathematical models [7–10], and discrete element method (DEM) [11, 12], have been applied to quantitatively capture the information of the burden during the charging process. Among these methods, the mathematical model of burden distribution offers various advantages, including rigorous theoretical foundation and fast evaluation of the macro-profile of burden, which can be used for the online prediction of the burden distribution. In terms of DEM, the information on the particle scale can be captured, such as the velocity and position of each particle, the interaction between particles, and the formation and evolution of mixed layer. Therefore, the mathematical model and DEM are two popular methods, which are widely used to investigate the burden movement and distribution.

Recently, mathematical models for estimating the burden distribution have been developed and continuously improved. Fu et al. [9] divided the burden movement during the charging process into three parts and developed a mathematical model, consisting of three sub-models: burden trajectory model, burden profile model, and burden descending model. They proposed the nonuniform descending model and validated it using published experimental results, and the accuracy increased notably for the modified model with the nonuniform descending velocity compared with the original uniform descending model.

Saxén and Hinnelä [10] established a mathematical model to capture the burden behavior of the charging process and presented a detailed scheme for calculating the burden profile. The presentation of details of developing burden profile is of critical importance to improve the model considering the burden profile formed by previous rings, which requires a generic algorithm to handle arbitrary cases. Mitra and Saxén [8] illustrated that the mathematical model could analyze the effect of small changes in the charging program on the arising burden distribution, indicating that the model has the potential for designing a new charging program or optimizing the existing charging program. Park et al. [13] proposed a new repose angle model for the burden profile model, which was used for calculating the burden profile. The proposed model was validated by comparing the results of the model with those of a scaled model experiment and DEM simulation.

Although extensive efforts have been made to develop and improve the mathematical model for accurately evaluating the burden trajectory and distribution, there are still some simplified treatment of the burden trajectory model. For instance, the initial velocity of the burden when entering the feeding pipe and the velocity attenuation caused by collision between the burden and the rotating chute are difficult to be captured by the traditional physical experiments. Therefore, in previous studies, the initial velocity was neglected [8–10] or calculated using the hydraulic continuity equation [6, 14], and the velocity attenuation factor due to the collision was treated as an invariant constant [13, 15, 16]. However, these simplification processes affect the accuracy of the model, which needs to be further improved. With the emergence and development of DEM, the ironmaking in the blast furnace was widely investigated [17–19]. Mio et al. [4, 5] carried out a 1/3-scale physical experiment and verified that the DEM simulation of the charging process was highly reliable when used for the predictions of burden trajectory and distribution in the blast furnace. Thus, DEM is a good choice to analyze the initial velocity and velocity attenuation. In addition, the stock line is an important operation parameter for the charging of the blast furnace. Our previous results [20] showed that the change in stock line could cause the changes in the burden profile and distribution, which further caused the fluctuation of furnace operating conditions. In the actual production, the stock line frequently fluctuates, and even the low stock line occurs due to the sudden slip of the burden. Adjusting chute angles is necessary to address the large fluctuation of stock line or have a low stock line for stabilizing the burden distribution. Despite the marked importance of treating the fluctuation of the stock line, there are only few studies that focus on this.

Based on the aforementioned reviews, a DEM model of charging and a mathematical model of burden distribution were developed to improve the burden trajectory model for accurately calculating the burden trajectory and cope with the fluctuation of the stock line for stabilizing the burden distribution and operating conditions, respectively. In this study, the initial velocities of the pellet, sinter and coke when entering the feeding pipe with different diameters and different openings of the throttle valve were calculated using the DEM model. Similarly, the velocity attenuation factors of the three kinds of particles under different chute angles were analyzed using the velocities before and after collision, which were captured by the DEM model. The initial velocity and velocity attenuation factor were applied to improve the burden trajectory model, and the accuracy increased notably by comparing with that for the original model. Besides, based on the improved mathematical model, a scheme for rectifying the chute angles was proposed to address the fluctuation of the stock line. The validity of the scheme was confirmed through the calculated results of burden distribution under different stock lines from the mathematical model. The mathematical model has been successfully applied to evaluate the online burden distribution and cope with the fluctuation of the stock line.

2 Numerical methods

Bell-less top charging systems, including the parallel and serial hoppers, are widely used to tune burden distribution because of their high flexibility. Both charging systems have their advantages and disadvantages. The charging system with a serial hopper is considered as potential equipment because it would not cause the circumferential mass segregation of the burden when used for charging. Therefore, we considered it as the modeling object in the study. Figure 1 shows the geometric model of a 1080 m³ blast furnace in China. A three-dimensional charging model of the blast furnace using DEM was established to analyze the initial velocity and the velocity attenuation factor, as shown in Fig. 2. Based on the DEM model, the movement of the burden during the charging process includes five fundamental steps: (1) the burden with an initial velocity is accelerated to fall into the feeding pipe when charged from the hopper; (2) the burden falls to the rotating chute, and the collision between the burden and the rotating chute occurs and causes the velocity attenuation of the burden; (3) the burden slides along the chute and freely falls from the end of the chute as the chute rotates; (4) near the falling point of the burden, new burden surface profile forms based on the previous burden surface; and (5) the burden layer descends with ore reduction and coke

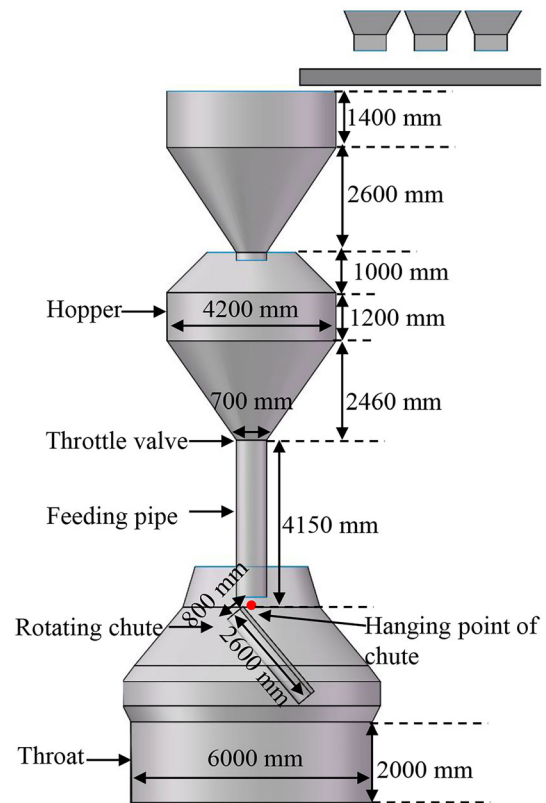


Fig. 1 Geometric model used in simulation

consumption. According to the charging process, the mathematical model was developed to evaluate the burden distribution, as shown in Fig. 2. This includes three sub-models: the burden trajectory model that describes the burden movement in steps (1)–(3), the burden profile model corresponding to step 4, and the burden descending model corresponding to step 5.

2.1 Mathematical model

2.1.1 Burden trajectory model

Figure 3 presents the schematic of the burden movement from the hopper to burden surface. The burden from the throttle valve at velocity v_0 falls into the feeding pipe and then collides with the chute. After the collision, the burden velocity perpendicular to the chute is reduced to zero, and burden velocity parallel to the chute has the attenuation. Subsequently, the burden slides down on the chute at velocity v_1 , gets into the freeboard in the furnace, and moves downward along a parabolic path at a velocity of v_2 . The calculations of these velocities and the falling point of the burden have been derived and described in detail in our previous studies [16, 21]. In this study, for simplicity, the calculated formulas of the velocities and falling point are directly provided. Velocity v_0 was obtained using the DEM

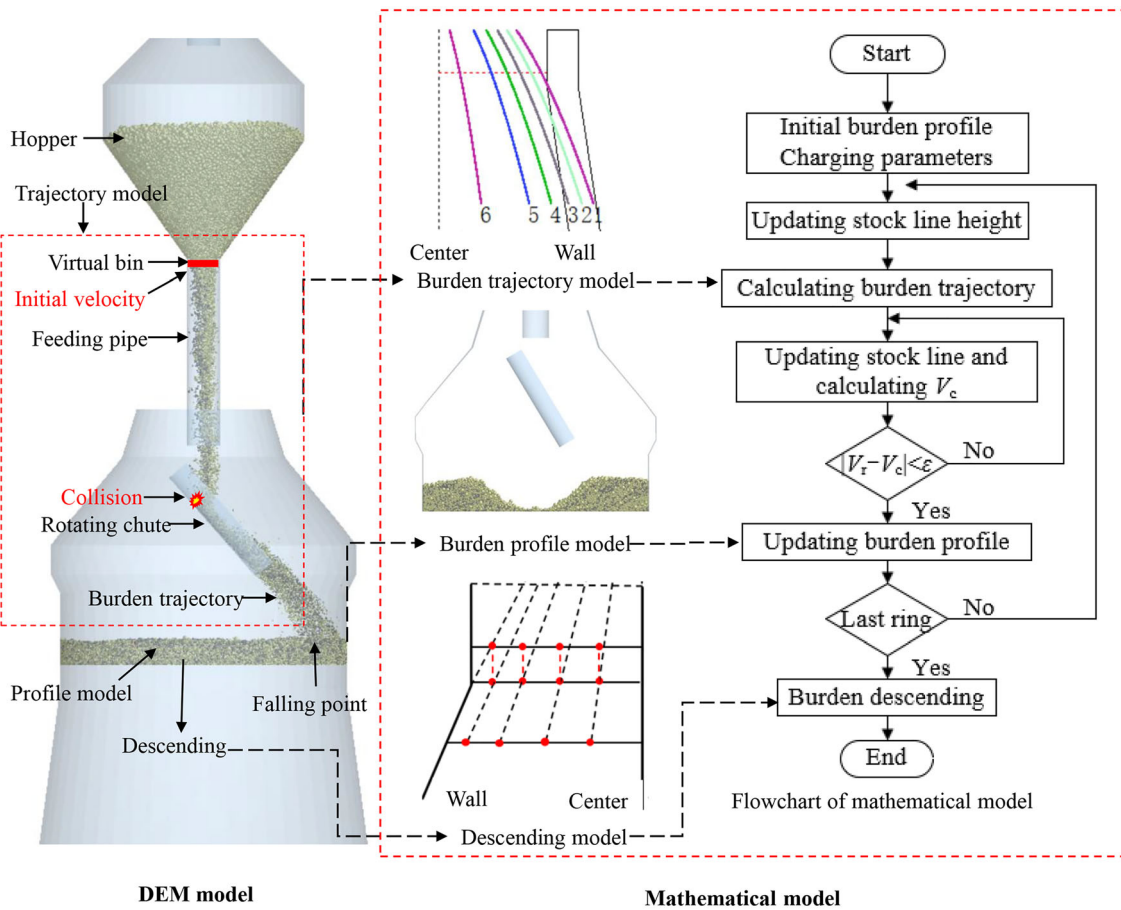


Fig. 2 DEM and mathematical models

model in Sect. 3.1. Velocities v_1 and v_2 can be calculated using Eqs. (1) and (2), respectively. Velocity attenuation coefficient k expressed in Eq. (1) was treated as a constant in the previous model [14, 15, 22], and its value was not clearly given. Velocity attenuation factors of the three kinds of particles were analyzed using the velocity before and after collision captured by the DEM model in Sect. 3.2 to clarify the velocity attenuations of the pellet, sinter, and coke from the collision. Velocity v_2 was introduced to Eq. (3) to calculate the falling point of the burden. The falling point is calculated based on an assumption that the stock line is not affected by the present dump and burden descent. This assumption would lead to about 6% error. In future, the effects of present dump and burden descent on the stock line should be considered to reduce the error. Based on the above analysis, accurate descriptions of the initial velocity and velocity attenuation factor are conducive to improving the computational accuracies of the velocity and falling point and further increase the reliability of calculating burden distribution.

$$v_1 = k \cos \alpha \sqrt{v_0^2 + 2g(H_0 + e/\sin \alpha)} \tag{1}$$

$$v_2 = \sqrt{2g(\cos \alpha - \mu \sin \alpha)l_\beta + 4\pi^2\omega^2l_\beta^2(\sin^2 \alpha - \sin \alpha \cos \alpha) + v_1^2} \tag{2}$$

$$L = \sqrt{(l_\beta \sin \alpha + v_2 \sin \alpha t)^2 + (l_\beta \omega \sin \alpha t)^2} \tag{3}$$

2.1.2 Burden profile model

With the rotation of the chute, the burden falls to form a new burden heap, and the shape was treated as triangular in the literature [8, 9, 23], as shown in Fig. 4a. The cross section of the heap was determined by the inner angle of repose φ_{in} and the outer angle of repose φ_{out} . Shi et al. [23] evaluated the accuracy of six existing repose angle models, in which all models predicted the burden profile well, and a certain model exhibited an increased accuracy for a particular case. Therefore, in the study, φ_{in} was regarded as constant, and φ_{out} was calculated by a linear function of the chute angle [9]. The formation process of burden profile in the model is

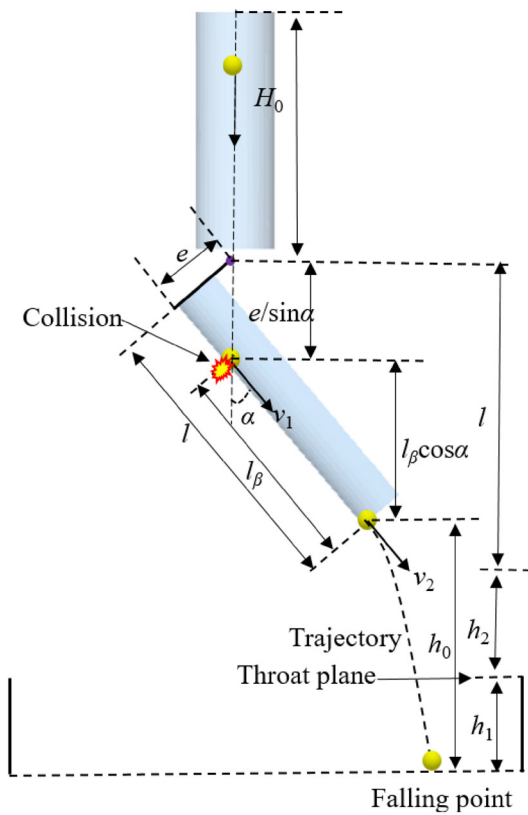


Fig. 3 Schematic illustration of burden movement from hopper to burden surface

shown in Fig. 4. New burden profile $f_2(r)$ was obtained by combining the falling point and repose angle model, as shown in Fig. 4b, c, which was calculated as follows:

$$\left| V_r - \int_0^R 2\pi r(f_2(r) - f_1(r))dr \right| < \varepsilon \quad (4)$$

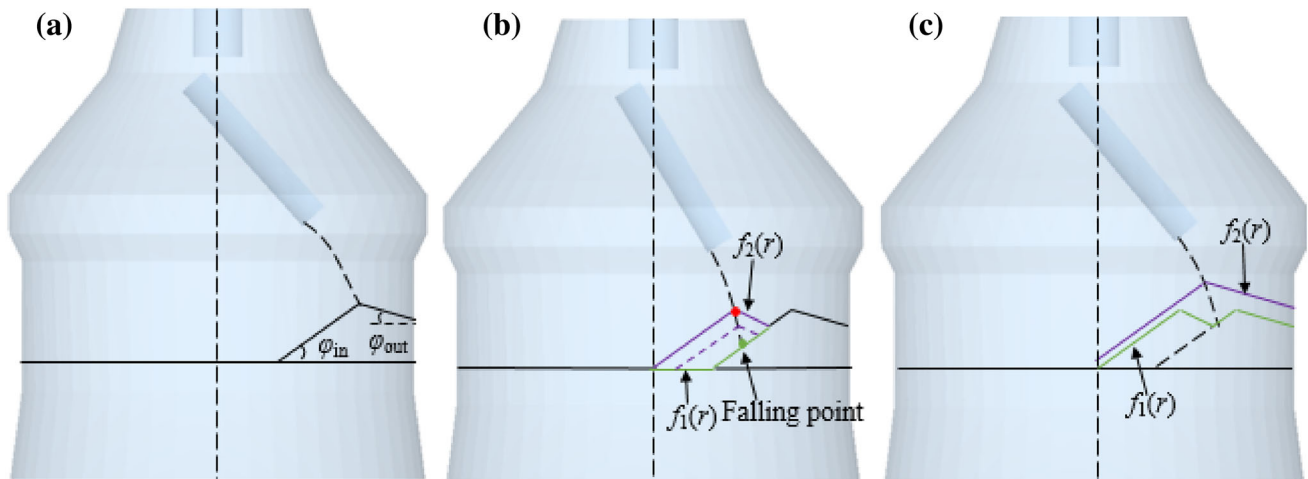


Fig. 4 Formation process of burden profile in mathematical model. **a** Shape of heap; **b** new burden profile; **c** next round charging

2.1.3 Burden descending model

Burden descending model was applied to predict the whole burden structures in the shaft. Nishio and Ariyama [24] developed the original burden descending model in 1982, assuming that the velocity of the burden in a vertical direction was uniform. Based on the linear hypothesis of the burden descending velocity in the vertical direction, Kajiwara et al. [25] firstly proposed the nonuniform descending model, and Fu et al. [9] introduced the relative velocity factor in this model to improve its accuracy. Zhou et al. [26] established an evaluation method to estimate the error between experimental result and the calculated one from above models. They found that all models could capture the main profile, and the uniform descending model might be the first option for roughly predicting burden structure due to its easier understanding and calculation. Therefore, the uniform descending model was applied to predict the structure of burden layer in the shaft. The detailed derivation process of the model was described in the literature [9, 24]. Based on the three sub-models and the flowchart shown in Fig. 2, there are mainly four fundamental steps: (1) input simulation parameters, which include some geometry parameters of blast furnace, charging parameters, initial burden profile and charging matrix; (2) calculate the falling point and burden trajectory; (3) calculate the critical volume and update burden profile; and (4) calculate the burden structure in the shaft by the burden descending model. The mathematical model was developed using the programming language Visual Basic using a graphical user interface (GUI).

2.2 DEM model

DEM is a popular numerical method used for describing the interactions between particles, which consist of the translational and rotational motions. The motions of the particle are calculated by Newton’s second law, and the interactions between particles are described by the non-linear Hertz–Mindlin no-slip model [27]. The governing equations and contact model are described in detail in previous work [28]. EDEM commercial software (EDEM™, England) was used for predicting the movement and distribution of the burden. Physical parameters of the pellet, sinter, and coke are shown in Table 1. The densities of the pellet and sinter were measured by a drainage method, and their friction coefficients were calibrated by the experiment of the repose angle that has been described in our previous paper [28]. Other parameters in Table 1 were taken from the literature [27, 29, 30]. Particle information used in simulation for analyzing the initial velocity of the particle flow is presented in Table 2.

3 Improved mathematical model and its application

3.1 Initial velocity of burden entering feeding pipe

The burden starts to be discharged from the hopper at a certain initial velocity after the throttle valve is opened. In the previous studies, the initial velocity of the burden when entering the feeding pipe was not considered in some literatures [8–10] or calculated using the hydraulic continuity equation [6, 14]. These might cause large calculation error regarding the initial velocity. According to the previous models [6, 14], the initial velocity was affected by the opening of the throttle valve and diameter of the feeding

Table 2 Particle information used in DEM simulation

Type	Diameter/mm	Mass ratio/%	Number
Pellet	10–12	23.5	107,596
	12–14	50.0	141,025
	14–16	26.5	48,583
Sinter	5–10	18.4	162,831
	10–16	28.5	91,935
	16–25	20.3	22,455
	25–40	32.8	10,789
Coke	25–40	20.5	51,758
	40–50	38.2	10,332
	50–75	41.3	6560

pipe. The throttle valve is located under the hopper as shown in Fig. 1. Figure 5a, b shows the actual structure and schematic diagram of the throttle valve, respectively. Therefore, to clarify the initial velocity of the burden under different openings of the throttle valve and diameters of the feeding pipe and improve the burden trajectory model, the DEM model in Fig. 2 was used to calculate the initial velocities of the pellet, sinter and coke. A virtual bin located at the outlet of the hopper in the DEM model was applied to capture the average velocity of particles in it. The average velocity was considered as the initial velocity of the burden discharging from the hopper.

Figure 6a–c presents the initial velocity of the pellet, sinter, and coke under different openings of the throttle valve and diameters of the feeding pipe, respectively. As shown in Fig. 6a, as the opening of the throttle valve and diameter of the feeding pipe increased, the initial velocity of the pellet increased, and the discharging outlet area increased. The proportion of the central high-speed particle flow area in the cross section of the layer increases with the increase in the discharging outlet area. Therefore, the initial

Table 1 Physical and contact parameters used in DEM simulation

Parameter	Pellet		Sinter		Coke		Wall
Density/(kg m ⁻³)	3674 [28]		3199 [28]		1050 [27]		7800
Poisson’s ratio	0.24 [27]		0.25 [29]		0.22 [27]		0.3
Shear modulus/Pa	1 × 10 ⁸ [28]		1 × 10 ⁸ [28]		2.21 × 10 ⁸ [27]		7 × 10 ⁸
Static friction coefficient	Pellet	0.4	Sinter	0.6	Coke	0.43 [30]	–
	Wall	0.36 [27]	Wall	0.52 [27]	Wall	0.5 [27]	
Rolling friction coefficient	Pellet	0.1	Sinter	0.24	Coke	0.46 [27]	
	Wall	0.16 [27]	Wall	0.2 [31]	Wall	0.15 [30]	
Restitution coefficient	Pellet	0.42 [27]	Sinter	0.35 [27]	Coke	0.39 [27]	
	Wall	0.62 [27]	Wall	0.4 [27]	Wall	0.42 [27]	
Time step/s	6.5 × 10 ⁻⁵		5 × 10 ⁻⁵		3.9 × 10 ⁻⁵		–

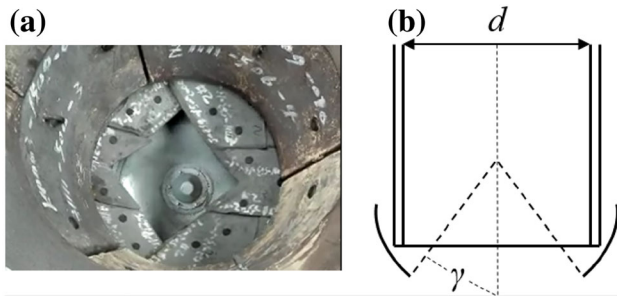


Fig. 5 Structure of throttle valve. **a** Actual object; **b** schematic diagram [21]

velocity of the pellet increased with the above two factors. Based on the data in Fig. 6a, the velocity was fitted as a binary linear function of the above two variables, as shown in Eq. (5), to obtain the initial velocity of the pellet under any opening and diameter. The correlation coefficient of

the regression equation was 0.977. Similarly, as shown in Fig. 6b, c, the variation trends of the initial velocities of the sinter and coke with the opening and diameter were consistent with that of the pellet. The initial velocities of the sinter and coke were also fitted as a linear function of the opening and diameter and calculated using Eqs. (6) and (7), respectively. Correlation coefficients of the regression equations of the sinter and coke were 0.957 and 0.976, respectively. The results suggest that the initial velocity in Eq. (1) for different types of burden could be calculated using the regression equation. Various researchers [4, 5, 32, 33] have verified the validity of DEM simulation in which it could reliably predict the burden trajectory and distribution of the blast furnace, indicating that the initial velocity of the burden from the DEM simulation was highly reliable. Hence, compared to the results ignoring the initial velocity or using hydraulic continuity equation for

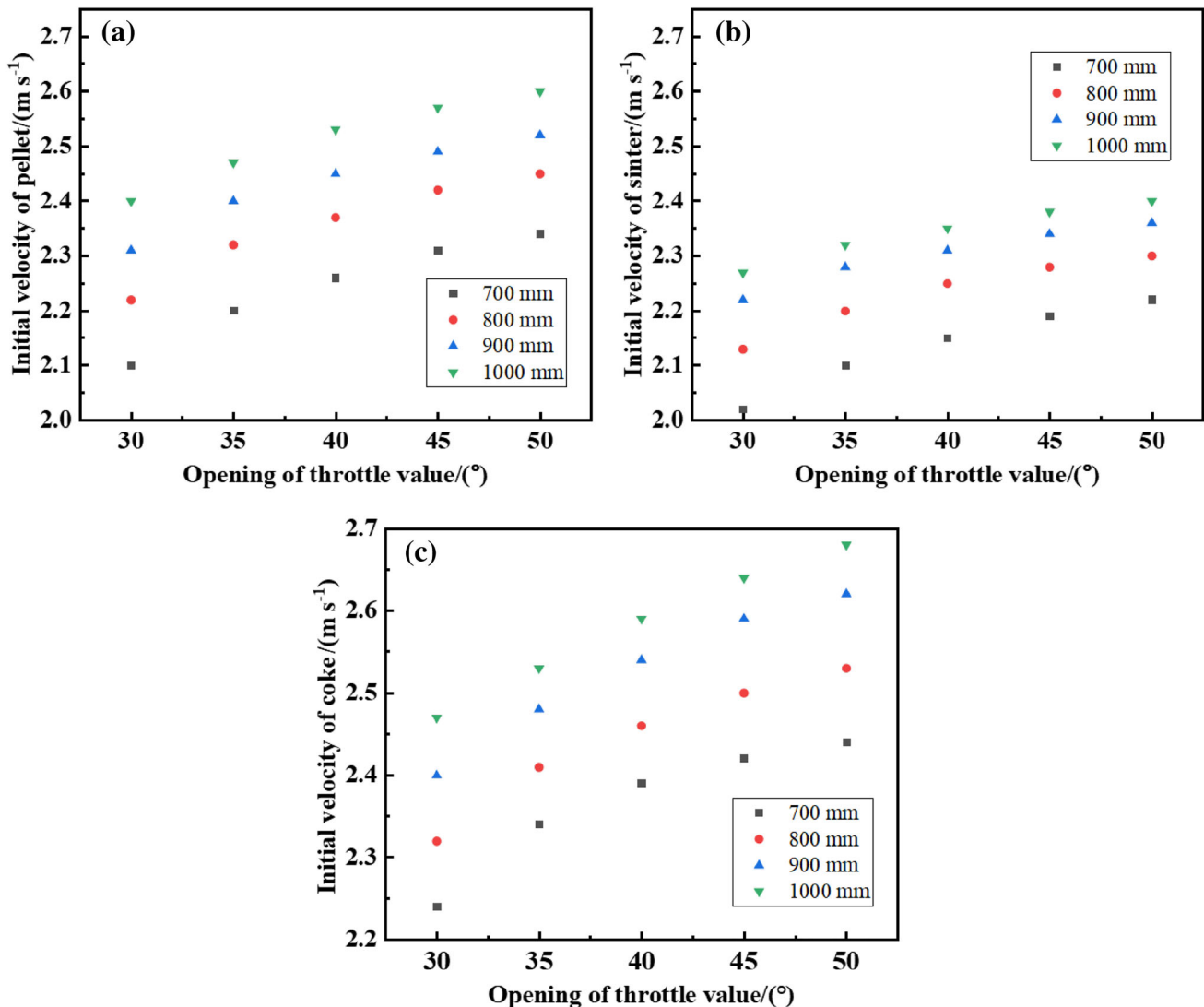


Fig. 6 Initial velocity of burden entering feeding pipe. **a** Pellet; **b** sinter; **c** coke

calculation, we considered that the results of the initial velocity from DEM simulation can be more reasonable or reliable. Concurrently, the initial velocity of different types of the burden was different, as shown in Fig. 6. Under the same condition, the initial velocity of the sinter was smaller than that of the pellet, which might be caused by the difference of the particle surface. Compared to the pellet, the sinter has a rougher surface and larger static friction coefficient, and the friction resistance between sintered particles was larger. Consequently, the interaction between sinter particles during the initial discharging process consumed more energy than that between pellet particles, and the initial velocity of the sinter was smaller. In terms of the initial velocity, coke was slightly higher than pellet under the same condition although coke has a larger static friction coefficient than pellet in Table 2. This is because the diameter of the coke was much larger than that of the pellet. When opening the throttle valve, the number of contact pairs between coke particles was much smaller than that between pellet particles. Therefore, the interaction between coke particles consumed less energy than that between pellet particles, and the initial velocity of the coke was larger.

Initial velocity of the burden:

$$\text{Pellet: } v_{0P} = 1.195 + 0.0108\gamma + 8.94 \times 10^{-4}d \quad (5)$$

$$\text{Sinter: } v_{0S} = 1.35 + 0.00785\gamma + 6.94 \times 10^{-4}d \quad (6)$$

$$\text{Coke: } v_{0C} = 1.445 + 0.0103\gamma + 7.3 \times 10^{-4}d \quad (7)$$

3.2 Velocity attenuation caused by collision between burden and chute

Burden collides with the rotating chute after leaving the feeding pipe, as shown in Fig. 7. The value and direction of the burden velocity are changed because of the collision. Before the collision, as shown in Fig. 7a, the velocity of the particle v_b could be divided into the velocity of the particle perpendicular to the chute direction v_{bv} and the velocity of the particle parallel to the chute direction v_{bp} . Previous studies [10, 13, 15, 16] reported that, after the collision, v_{bv} decreases to 0 m/s, and v_{bp} would attenuate to some extent. Correction coefficient k was introduced to represent the attenuation of the velocity caused by the collision. k was considered as a constant in the previous burden trajectory models. However, the calculated result showed that the particle collided with the chute at an angle of β to the vertical direction of the chute, as shown in Fig. 7b. After collision, the particle moved to the opposite direction at the same angle, and the velocity of the particle parallel to the chute direction v_1 was $v_c \cos \alpha$. k was defined

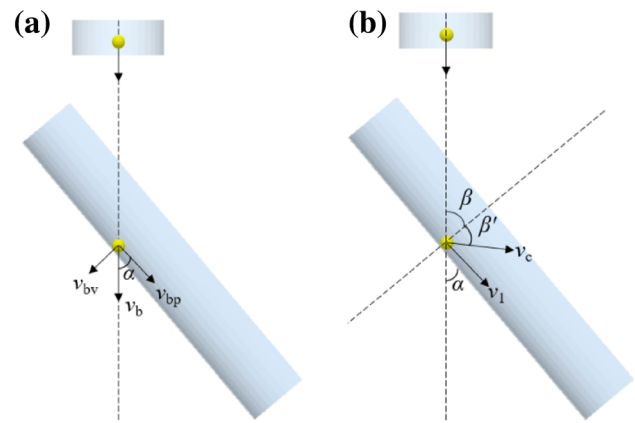


Fig. 7 Collision between particle and rotating chute. **a** Before collision; **b** after collision

as the ratio of v_1 to v_{bp} in current model, which could be calculated using Eq. (8).

$$k = \frac{v_1}{v_{bp}} = \frac{v_c \cos \alpha}{v_b \cos \alpha} = \frac{v_c}{v_b} \quad (8)$$

where v_b and v_c are the velocities of the particle before and after the collision, respectively, which could be captured by DEM simulation. Meanwhile, the fact that the degree of velocity attenuation is directly related to the chute angle is worth noting. Based on this idea, we need to investigate the velocity attenuations of the pellet, sinter and coke caused by the collision under different chute angles using the developed DEM model and to improve the accuracy of the burden trajectory model. Since the burden trajectory model was established based on the movement of a single particle [9], the velocity attenuation of a single particle was captured in our investigation. We found that the diameter of the burden has no influence on the velocity attenuation by numerical simulation. Hence, medium-size particles were selected as research objects. Under the normal charging of a blast furnace, the chute angle is between 20° and 45°. The chute angle in the model was set as 20°, 25°, 30°, 35°, 40°, and 45°.

Tables 3–5 present the velocities of pellet, sinter, and coke before and after collision and the corresponding attenuation coefficient. As shown in Fig. 7, the falling height of particle slightly decreases with the increase in the chute angle. Consequently, in Table 3, with the increase in the chute angle from 20° to 45°, v_b decreased from 11.47 to 10.40 m/s, and v_c decreased from 9.01 to 5.71 m/s. Compared with v_b , the increasing extent of v_c was approximately three times. k is also reduced from 0.79 to 0.55, which confirms the previous idea that the chute angle is directly related to the degree of the velocity attenuation. The attenuation coefficient of pellet was fitted as a linear

Table 3 Velocity of pellet before and after collision and its attenuation coefficient

$\alpha/(\circ)$	20	25	30	35	40	45
$v_b/(\text{m s}^{-1})$	11.47	11.07	10.82	10.63	10.50	10.40
$v_c/(\text{m s}^{-1})$	9.01	8.03	7.25	6.61	6.04	5.71
k	0.79	0.72	0.67	0.62	0.58	0.55

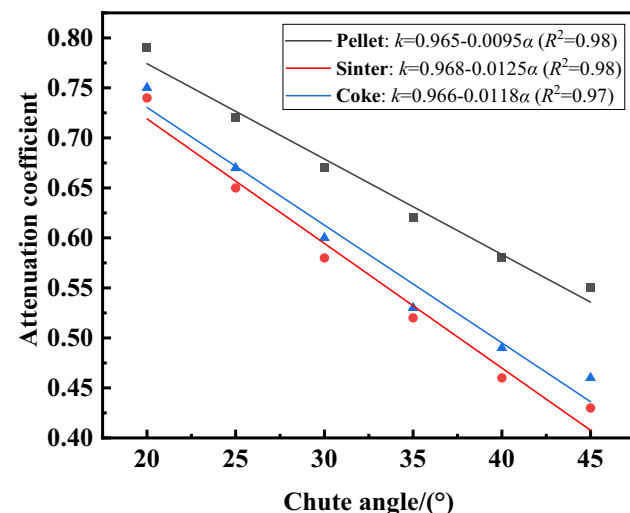
Table 4 Velocity of sinter before and after collision and its attenuation coefficient

$\alpha/(\circ)$	20	25	30	35	40	45
$v_b/(\text{m s}^{-1})$	11.39	11.03	10.79	10.60	10.47	10.36
$v_c/(\text{m s}^{-1})$	8.43	7.16	6.23	5.57	4.79	4.49
k	0.74	0.65	0.58	0.52	0.46	0.43

Table 5 Velocity of coke before and after collision and its attenuation coefficient

$\alpha/(\circ)$	20	25	30	35	40	45
$v_b/(\text{m s}^{-1})$	11.48	11.10	10.84	10.65	10.50	10.40
$v_c/(\text{m s}^{-1})$	8.61	7.42	6.50	5.64	5.14	4.83
k	0.75	0.67	0.60	0.53	0.49	0.46

function of the chute angle, as shown in Fig. 8, and the determination coefficient of the regression equation was 0.98. Simultaneously, the changes in attenuation coefficients of sinter and coke in Tables 4 and 5 with the chute angle were similar to that of the pellet, and the attenuation coefficients of sinter and coke were also fitted as a linear function of the chute angle, respectively, as shown in Fig. 8. Regression equations of three particles in Fig. 8

**Fig. 8** Effect of chute angle on attenuation coefficient. R^2 —Determination coefficient

were introduced into Eq. (1) to correct the calculation of particle velocity. Velocities at which the pellet, sinter, and coke starts to move on the chute could be calculated by the improved Eqs. (9)–(11), respectively.

$$v_{1P} = (0.965 - 0.0095\alpha) \cos \alpha \sqrt{v_{0P}^2 + 2g(H_0 + e/\sin \alpha)} \quad (9)$$

$$v_{1S} = (0.968 - 0.0125\alpha) \cos \alpha \sqrt{v_{0S}^2 + 2g(H_0 + e/\sin \alpha)} \quad (10)$$

$$v_{1C} = (0.966 - 0.0118\alpha) \cos \alpha \sqrt{v_{0C}^2 + 2g(H_0 + e/\sin \alpha)} \quad (11)$$

3.3 Comparison between original trajectory model and improved one

The initial velocities and attenuation coefficients were applied to improve the burden trajectory model. Taking the sinter as an example, the differences between the original trajectory model and the improved model were compared. Table 6 presents the charging parameters of the blast furnace. Figure 9 provides comparisons of the sinter trajectory of previous six chute angles with the original, improved and DEM models. Sinter trajectories from the original and

Table 6 Charging parameters of blast furnace

D_0/m	h_1/m	H_s/m	$\beta_s(^{\circ})$	H_0/m	l/m	e/m	h_2/m
6	2	12.6	83	4.15	2.6	0.8	0.25
$\rho_o/(kg\ m^{-3})$	$\rho_c/(kg\ m^{-3})$	w_o/kg	w_c/kg	$\omega/(r\ min^{-1})$	μ_s	μ_c	k
1800	530	8800	36,000	8	0.52	0.52	0.8

improved models were different when chute gears were at 1, 2, and 3 (corresponding to the chute angles of 45°, 40°, and 35°, respectively), as shown in Fig. 6a, b, and they were approximate when the chute gears were at 4, 5, and 6 (corresponding to the chute angles of 30°, 25°, and 20°, respectively). Above results might be caused by the differences of the attenuation coefficients used in the original and improved models. Attenuation coefficient used in the original model was constant at a value of 0.8, and the coefficient used in the improved model is listed in Table 4. The difference of the attenuation coefficients between the original and improved models increased as the chute angle increased, widening the gap between the sinter trajectory calculated by the original and improved models. Figure 9c provides the sinter trajectories of the six chute angles calculated by DEM simulation. Results calculated using DEM model were compared with those of the original and improved models, indicating that the sinter trajectories from the improved model were in good agreement with that from DEM model. For quantitatively analyzing the differences between models, falling points of the sinter at the 2 m stock line calculated by the different models were compared, as shown in Table 7. The result of DEM model was used to evaluate the calculation errors of the original and improved models. Table 7 shows that falling points of the sinter calculated using the improved model were consistent with those calculated using DEM model, and the difference between falling points calculated using original model and DEM model increased as the chute angle increased. When the chute angle was 45°, the error of the original model was up to 12.04%, significantly decreasing the accuracy of the mathematical model of burden distribution. The error of the improved model was less than 2%, which suggests that the accuracy increased notably using the improved mathematical model with the velocity attenuation coefficients when compared with the original model.

3.4 Correcting chute angle to cope with low stock line

3.4.1 Attenuation scheme of chute angle

Low stock line is a common abnormal condition of the blast furnace, which occurs when the height of the stock line was lower than the specified stock line by more than 0.5 m, and this condition can last for more than 1 h [34].

When the low stock line occurred, the particle flow can easily collide with the furnace wall, as shown in the original burden trajectory in Fig. 10. This collision between the particle flow and the furnace wall destroys the normal burden distribution and gas distribution, deteriorating the pre-heating and pre-reduction of the burden in the shaft and further affecting the reduction in ore and gas distribution in the lower part of the blast furnace. Therefore, the chute angle must be adjusted to avoid the collision, and the attenuation scheme of chute angle needs to be provided.

The blue trajectory was the original burden trajectory at a certain chute angle, as shown in Fig. 10. The falling point of the burden corresponding to the chute angle was located at the position 1 when the burden surface was located at the specified stock line. When the blast furnace was in normal production, based on the uniform descending model [8], the burden at position 1 descended along the dotted line in Fig. 10. The burden was located at position 3 after descending to height H_d along the vertical direction of the blast furnace. However, the factors, such as frequent collapsing, slipping after hanging or untimely supply of the burden, may cause the burden surface located at the position of the low stock line, as shown in Fig. 10. If the situation of the low stock line does not occur, the burden at position 1 will descend along the path-line to position 3. Therefore, we selected position 3 as the new falling point to correct the chute angle when this situation occurs. The radial coordinates of position 3 was calculated using Eq. (12). The attenuation scheme of the chute angle was changed into a mathematical problem: to find the chute angle corresponding to the falling point of the burden at position 3 when the height of stock line was $H_h + H_d$. There is only one chute angle in the range of 0°–90°, which corresponds to the new falling point and new burden trajectory in Fig. 10. To solve the above problem, the dichotomy, as shown in Fig. 11, was used to determine the new chute angle.

$$L' = L + H_d / \tan(\beta_s) \tag{12}$$

3.4.2 Correcting chute angle for stabilizing burden distribution

The charging matrices of ore and coke in a 1080 m³ blast furnace are $O_{3,3,3,3,2}^{42,40,38,35,31}$ and $C_{3,3,3,3,2}^{41,39,37,34,30,25}$ (The

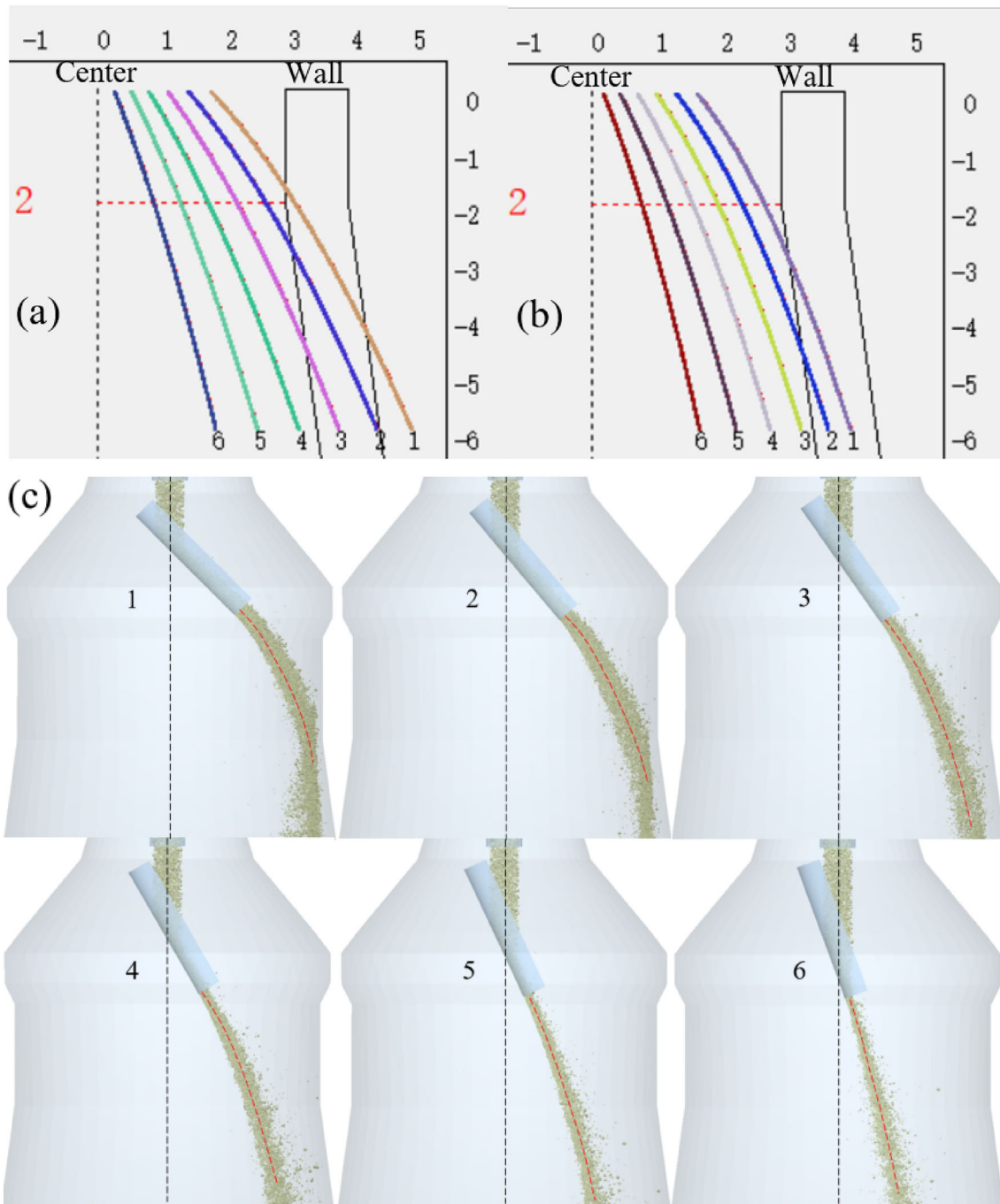


Fig. 9 Sinter trajectory. **a** Original model; **b** improved model; **c** DEM model

superscripts indicate the angle of chute at different gears, and subscripts represent the corresponding number of charging rings), respectively. In Sect. 3.3, Table 6 lists the charging parameters of the blast furnace, and the height of the specified stock line was 1.4 m. The improved burden trajectory model was used to calculate the burden trajectory. The burden structure of blast furnace consists of 75% sinter + 20% pellet + 5% lump. The ratio of lump is small, and thus the lump amount in the simulation is

ignored. The velocity attenuation coefficient of the ore was taken as the average weight of the sinter and pellet. Taking the low stock line of 3 and 4 m as examples, the availability of the attenuation scheme in maintaining the stable burden distribution was illustrated. Figure 12a, b presents the ore and coke trajectory under current charging matrices, respectively. The result showed that particle flows collided with the furnace wall when the stock line was 4 m. Figure 12c, d shows the burden profile and ratio

Table 7 Falling point of sinter calculated using different models

$\alpha/(\text{°})$	20	25	30	35	40	45
Original model/m	0.84	1.26	1.7	2.15	2.61	3.07
Error of original model/%	2.4	3.3	5.6	5.9	7.85	12.04
Improved model/m	0.82	1.22	1.62	2.02	2.39	2.75
Error of improved model/%	0	0	0.6	0.5	1.2	0.4
DEM model/m	0.82	1.22	1.61	2.03	2.42	2.74

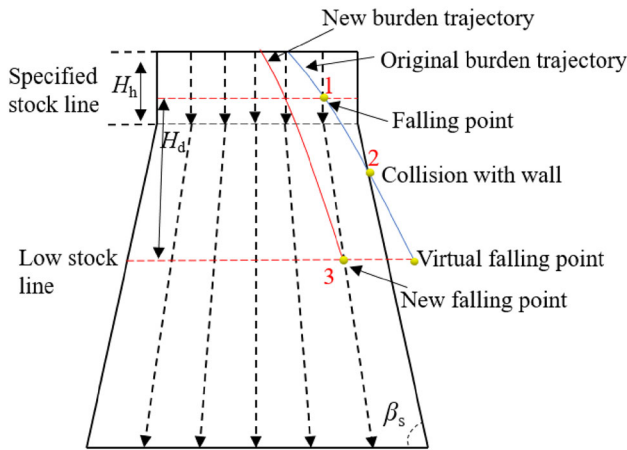


Fig. 10 Particle flow collide with furnace wall and new burden trajectory under low stock line

of ore to coke at a 1.4 m stock line, respectively. Figure 12e, f presents the burden profile and ratio of ore to coke at a 3 m stock line when the chute angle was not corrected, respectively. The burden distribution at 3 m stock line was different with that at a 1.4 m stock line. When the stock line was 4 m, the particle flows collided with the furnace wall, as shown in Fig. 12a, b. Predictably, there was a great difference in burden distribution between the 4 m and 1.4 m stock line. Therefore, whether the particle flow collided with the furnace wall or not, if the chute angle was not corrected, the normal burden distribution would be disturbed when a low stock line occurred.

Based on the attenuation scheme of the chute angle presented in Fig. 10, the chute angles of the 3 m and 4 m stock lines after attenuation were calculated using the algorithm shown in Fig. 11. Tables 8 and 9 provide the chute angles of 3 m and 4 m stock lines under different charging gears after attenuation, respectively. Figure 13a, c shows the burden profiles of 3 m and 4 m stock line after correcting the chute angle, respectively. Compared with the burden profile presented in Fig. 12c, there was only a small difference between the layer structures in Fig. 12c after correcting the chute angle. Figure 13b, d presents the radial distributions of the ratio of ore to coke of 3 m and 4 m

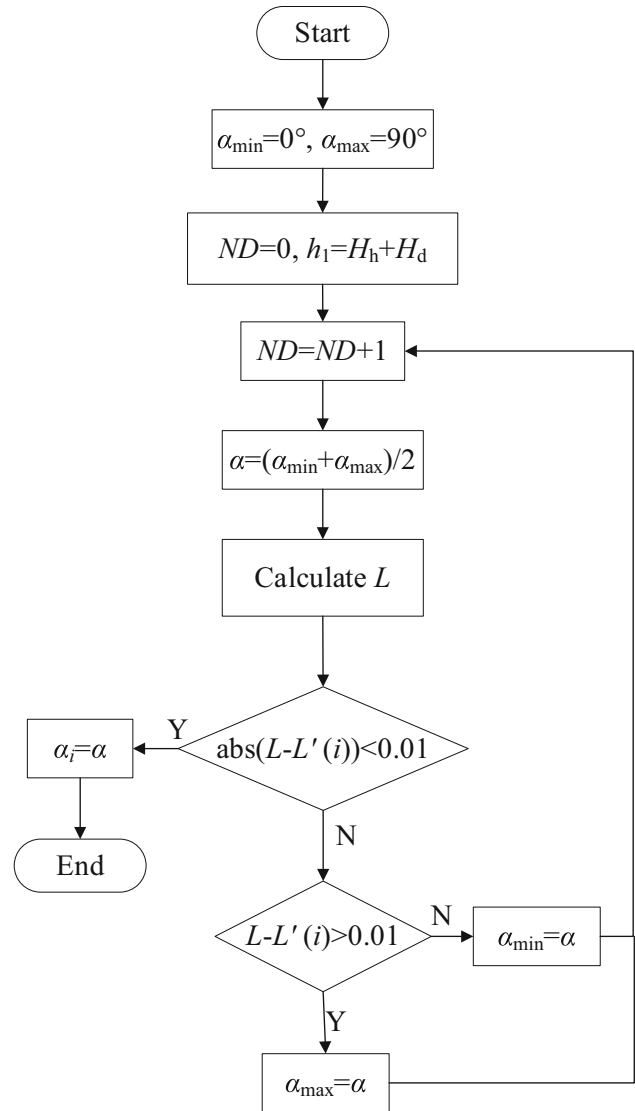


Fig. 11 Algorithm of correcting chute angle. *ND*—Number of iterations

stock lines after correcting the chute angle, respectively. The radial distributions were consistent with that in Fig. 12d. The analysis illustrated that the attenuation scheme of the chute angle proposed in the study could

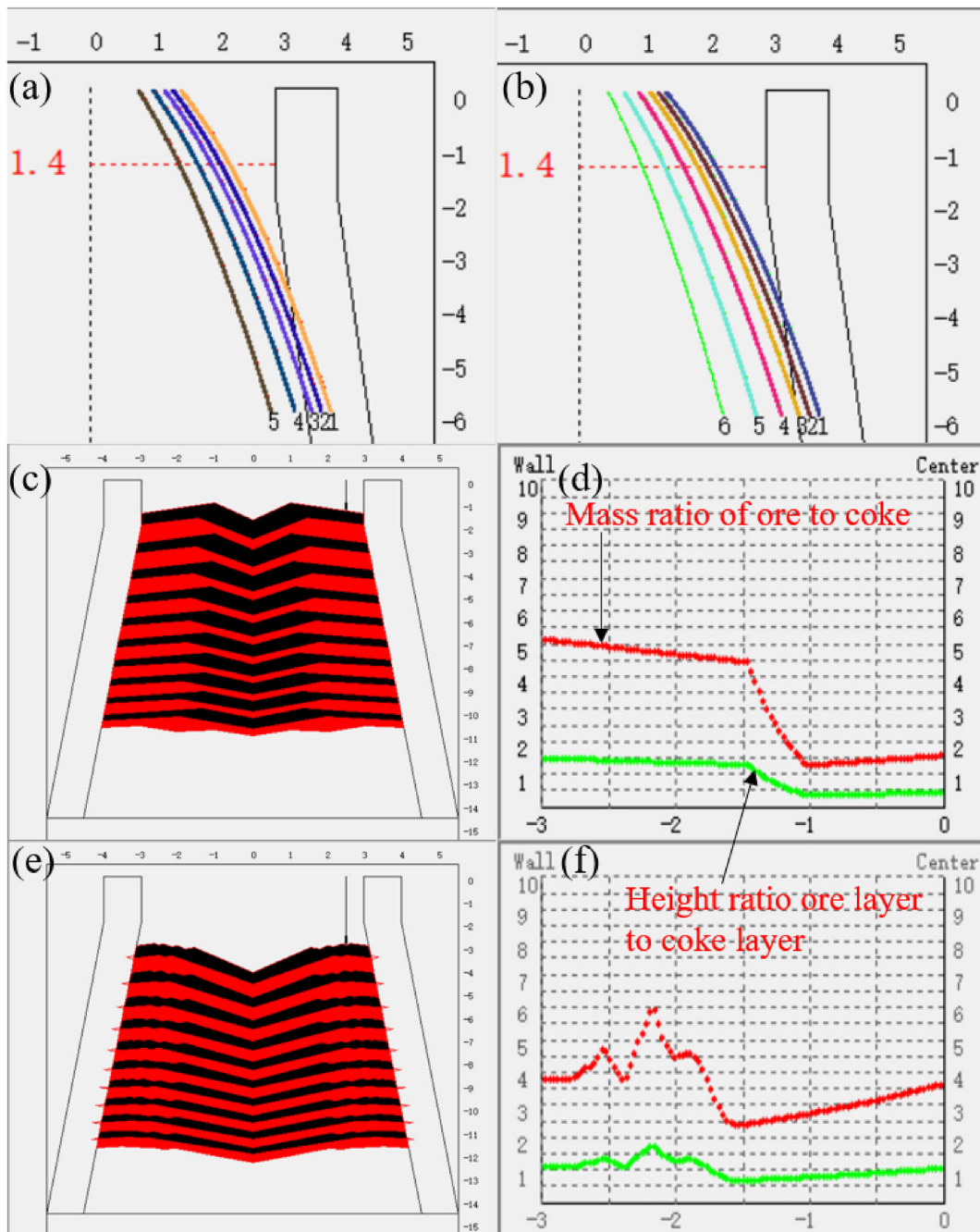


Fig. 12 Information of burden movement and distribution. **a** Ore trajectory; **b** coke trajectory; **c** burden profile of 1.4 m stock line; **d** ratio of ore to coke of 1.4 m stock line; **e** burden profile of 3 m stock line; **f** ratio of ore to coke of 3 m stock line

effectively solve the charging problem under the stock line and maintain the stable burden distribution of the blast furnace. Therefore, the attenuation scheme could be embedded in the charging control program, and the chute angle was automatically corrected based on the real-time measured height of the stock line to cope with the charging problem of the low stock line. The mathematical model of the burden distribution has been successfully applied to

evaluate the online burden distribution and address the fluctuation of the stock line.

4 Conclusions

1. The initial velocity of the burden entering the feeding pipe increased as the opening of the throttle valve and

Table 8 Chute angle of 3 m stock line after attenuation (°)

Gear	9	8	7	6	5	4
Ore	35.1	33.3	31.7	29.2	25.8	–
Coke	34.2	32.5	30.9	28.2	24.9	20.9

Table 9 Chute angle of 4 m stock line after correction (°)

Gear	9	8	7	6	5	4
Ore	32.6	31.1	29.5	27.2	24.1	–
Coke	31.8	30.2	28.7	26.4	23.3	19.6

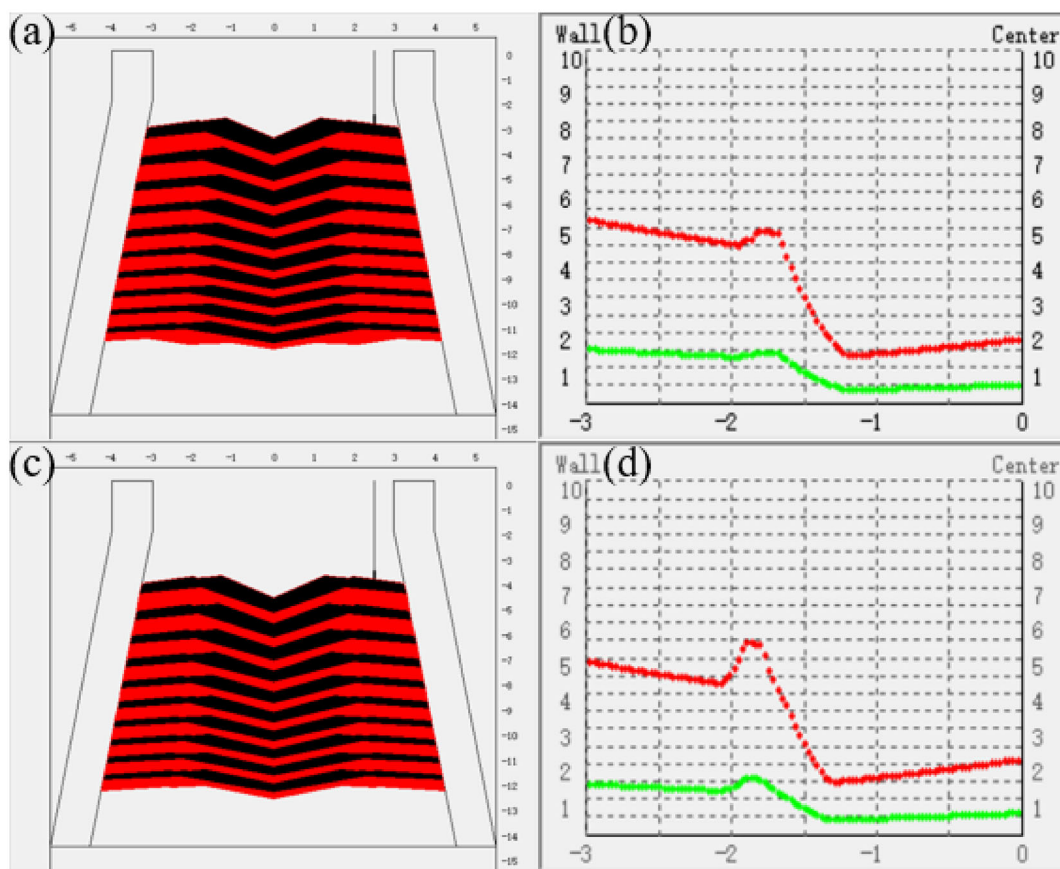


Fig. 13 Burden distribution after correction of chute angle. **a** Burden profile of 3 m stock line; **b** ratio of ore to coke of 3 m stock line; **c** burden profile of 4 m stock line; **d** ratio of ore to coke of 4 m stock line

the diameter of the feeding pipe increased. Besides, the differences of the diameter and friction coefficient of the burden caused a difference in the initial velocity of the burden under the same condition.

2. The change in the velocity during the collision between the particle and the chute was analyzed in

detail, and the velocity attenuation coefficient was redefined. The attenuation coefficient linearly decreased as the chute angle increased.

3. The result from the DEM model was used to evaluate the calculation errors of the original and improved models. The falling point error of the burden from the

original model was up to 12.04%, and that from the improved model was less than 2%. The result suggested that the accuracy increased notably using the improved model with the initial velocity and velocity attenuation coefficient.

4. Based on the burden descending path line, an attenuation scheme of the chute angle was proposed to cope with the charging problem of the stock line. The layer structure in the shaft and radial ratio of ore to coke after correcting the chute angle remained unchanged, indicating that the attenuation scheme could effectively solve the charging problem under the stock line and maintain the stable burden distribution. The mathematical model of burden distribution has been successfully applied to evaluate the online burden distribution and cope with the fluctuation of the stock line.

Acknowledgements The authors gratefully acknowledge the financial support from the China Minmetals Science and Technology Special Plan Foundation (2020ZXA01) and the National Natural Science Foundation of China (U1960205).

Declarations

Conflict of interest The authors declare that they have no known competing financial interests or personal relationships that could have appeared to influence the work reported in this paper.

References

- [1] S. Natsui, A. Hirai, K. Terui, Y. Kashihara, A. Murao, Y. Miki, H. Nogami, *Chem. Eng. J.* 427 (2022) 131484.
- [2] N. Standish, *Powder Technol.* 45 (1985) 43–56.
- [3] Y. Kajiwara, T. Jimbo, T. Joko, Y.I. Aminaga, T. Inada, *ISIJ Int.* 24 (1984) 799–807.
- [4] H. Mio, Y. Narita, K. Nakano, S. Nomura, *Processes* 8 (2019) 6.
- [5] H. Mio, Y. Narita, S. Matsuzaki, K. Nishioka, S. Nomura, *Powder Technol.* 344 (2019) 797–803.
- [6] Y.L. Yang, Y.X. Yin, D. Wunsch, S. Zhang, X.Z. Chen, X.L. Li, S.S. Cheng, M. Wu, K.Z. Liu, *ISIJ Int.* 57 (2017) 1350–1363.
- [7] J. Xu, S.L. Wu, M.Y. Kou, L.H. Zhang, X.B. Yu, *Appl. Math. Model.* 35 (2011) 1439–1455.
- [8] T. Mitra, H. Saxén, *Metall. Mater. Trans. B* 45 (2014) 2382–2394.
- [9] D. Fu, Y. Chen, C.Q. Zhou, *Appl. Math. Model.* 39 (2015) 7554–7567.
- [10] H. Saxén, J. Hinnelä, *Miner. Process. Extr. Metall. Rev.* 25 (2004) 1–27.
- [11] Y.W. Yu, H. Saxén, *Powder Technol.* 262 (2014) 233–241.
- [12] Y. Narita, H. Mio, T. Orimoto, S. Nomura, *ISIJ Int.* 57 (2017) 429–434.
- [13] J.I. Park, H.J. Jung, M.K. Jo, H.S. Oh, J.W. Han, *Met. Mater. Int.* 17 (2011) 485–496.
- [14] Y.W. Yu, C.G. Bai, Z.R. Zhang, F. Wang, D.G. Lv, C. Pan, *Ironmak. Steelmak.* 36 (2013) 505–508.
- [15] V.R. Radhakrishnan, K. Maruthy Ram, *J. Process Control* 11 (2001) 565–586.
- [16] H. Li, H. Saxén, W. Liu, Z. Zou, L. Shao, *Metals* 9 (2019) 1003.
- [17] Q. Li, R. Tang, S. Wang, Z.S. Zou, *Chem. Eng. J.* 433 (2022) 133529.
- [18] S. Natsui, K. Tonya, A. Hirai, H. Nogami, *Chem. Eng. J.* 414 (2021) 128606.
- [19] D.K. Chibwe, G.M. Evans, E. Doroodchi, B.J. Monaghan, D.J. Pinson, S.J. Chew, *Powder Technol.* 366 (2020) 22–35.
- [20] J.S. Chen, H.B. Zuo, J.X. Wang, Q.G. Xue, J.S. Wang, *J. Iron Steel Res. Int.* 30 (2023) 216–226.
- [21] J. Chen, H. Zuo, Q. Xue, J. Wang, *Powder Technol.* 398 (2022) 117055.
- [22] L. Shi, G. Zhao, M. Li, X. Ma, *Appl. Math. Model.* 40 (2016) 10254–10273.
- [23] P.Y. Shi, D. Fu, P. Zhou, C.Q. Zhou, *Ironmak. Steelmak.* 42 (2015) 756–762.
- [24] H. Nishio, T. Ariyama, *Tetsu-to-Hagane* 68 (1982) 2330–2337.
- [25] Y. Kajiwara, T. Jimbo, T. Sakai, *Trans. Iron Steel Inst. Jpn.* 23 (1983) 1045–1052.
- [26] P. Zhou, P.Y. Shi, Y.P. Song, K.L. Tang, D. Fu, C.Q. Zhou, *J. Iron Steel Res. Int.* 23 (2016) 765–771.
- [27] H. Wei, H. Nie, Y. Li, H. Saxén, Z.J. He, Y.W. Yu, *Powder Technol.* 364 (2020) 593–603.
- [28] J. Chen, H. Zuo, H. Zhao, Q. Xue, J. Wang, *Powder Technol.* 409 (2022) 117845.
- [29] H. Mio, M. Kadowaki, S. Matsuzaki, K. Kunitomo, *Miner. Eng.* 33 (2012) 27–33.
- [30] Y.W. Yu, H. Saxén, *Ind. Eng. Chem. Res.* 51 (2012) 7383–7397.
- [31] A. Tripathi, V. Kumar, A. Agarwal, A. Tripathi, S. Basu, A. Chakrabarty, S. Nag, *Powder Technol.* 380 (2021) 288–302.
- [32] Y.W. Yu, H. Saxén, *Steel Res. Int.* 84 (2013) 1018–1033.
- [33] Y.W. Yu, H. Saxén, *Ironmak. Steelmak.* 38 (2011) 432–441.
- [34] X.L. Wang, *Metallurgy of iron and steel (Ironmaking)*, 3rd Ed., Metallurgical Industry Press, Beijing, China, 2012.

Springer Nature or its licensor (e.g. a society or other partner) holds exclusive rights to this article under a publishing agreement with the author(s) or other rightsholder(s); author self-archiving of the accepted manuscript version of this article is solely governed by the terms of such publishing agreement and applicable law.